Difference of total precipitation and snowfall in the Upper Yangtze River basin under 1.5 °C and 2 °C global warming scenarios

Yanqun Ren[1,2,3] · Suxia Liu[1,3]

Abstract

The influence of climate change on regional-scale precipitation is becoming undeniable, and can lead to increased flood and drought risks in some regions. The study assessed the potential effect of global warming of 1.5 °C and 2 °C on total precipitation and snowfall in the Upper Yangtze River Basin (UYRB) based on General Circulation Models (GCMs). Seven total precipitation and six snowfall indices were employed in this analysis. The results show that the annual precipitation (PA) in the UYRB will increase by approximately 4.5–5% and 9–13% per 1.0 °C under the 1.5 °C and 2 °C warming, respectively. Spatially, the PA is shown to increase across the northern part of the basin, but decrease in the southern part. Relative to the baseline period (1986–2005), the frequency of trace and moderate precipitation days shows a decreasing trend, while that of heavy and intense precipitation days will increase under both 1.5 °C and 2 °C warming scenarios. Moreover, it varies among significance levels of trace, light, moderate, heavy and intense precipitation frequency under 1.5 °C and 2 °C warming for different Representative Concentration Pathways (RCPs). Unlike overall total precipitation, the annual snowfall (ASF) will decrease by approximately 2.5–8% per 1.0 °C under the 1.5 °C warming, and the 2–4% per 1.0 °C under the 2 °C warming. The ASF exhibits a decreasing trend in most of the UYRB except for the far northern part under all global warming scenarios. The date of first snowfall is modeled to be delayed and that of last snowfall will advance, which will lead to the decrease of snowfall days by about 15–20 days under different warming scenarios. In a warming world, total precipitation in the UYRB will increase and snowfall will decrease, which may increase the risk of flood in the future, and more attention should be paid.

1 Introduction

The global mean annual temperature (GMAT) increased over the last century (IPCC 2013), and this increase could have accelerated the evaporation of water, influenced the precipitation patterns, and affected ecological and human systems (Nelson et al. 2014; Su et al. 2017; Urry 2015). The Intergovernmental Panel on Climate Change (IPCC) has

✉ Suxia Liu
liusx@igsnrr.ac.cn

1 Key Laboratory of Water Cycle and Related Land Surface Processes, Institute of Geographic Sciences and Natural Resources Research, Chinese Academy of Sciences, Beijing, China

2 College of Surveying and Geo-Informatics, North China University of Water Resources and Electric Power, Zhengzhou, China

3 College of Environment and Resources/Sino-Danish Center, University of Chinese Academy of Sciences, Beijing, China

proposed that at the end of twenty-first century, the increase in GMAT would need to be less than 2 °C to support the normal operation of ecological and human systems. In recent years, however, many researchers have warned that expecting global warming to be limited to 2 °C of warming is overly optimistic (IPCC 2018; van Vliet et al. 2012), because global emissions are currently tracking at the high end of the plausible scenarios (Friedlingstein et al. 2014; Peters et al. 2012), warranting stringent limits on cumulative CO_2 emissions (Seneviratne et al. 2016). World leaders gathered in Paris in December 2015 for the 21st Conference of the Parties (COP21) of the United Nations Framework Convention on Climate Change (UNFCCC) and accepted that further steps needed to be taken to limit the increase in GMAT to well below 2 °C above pre-industrial levels and more efforts are needed to be pursued to limit the temperature increase to 1.5 °C above pre-industrial levels (Hulme 2016; IPCC 2013). Unlike that of the 2 °C GMAT warming, the 1.5 °C GMAT warming scenario is relatively unexplored, and studies highlighting its feasibility and impacts are only

beginning to emerge (Aerenson et al. 2018; Karmalkar and Bradley 2017; Mitchell et al. 2016; Seneviratne et al. 2018).

Climate change could affect regional hydrologic cycles significantly (Dore 2005; Khoi and Suetsugi 2014). Therefore, understanding the possible hydrological behavior under future climate change scenarios is important for effective water resource management (Elliott et al. 2014; Teutschbein et al. 2015). Because precipitation is the most important component of hydrological cycles (Harder and Pomeroy 2013), changes in precipitation are among the major consequences of global warming (Dore 2005). Research has shown that the global mean precipitation (GMP) response to a GMAT increase of 1 °C is an increasing in the range of 1–3% (Held and Soden 2006). Precipitation intensity is projected to increase by approximately 7.0% per 1.0 °C increase in GMAT, which is almost the same as the rate of change in atmospheric precipitable water (Sun et al. 2007; Trenberth et al. 2003). The precipitation change shows spatial differences throughout China, annual precipitation in the southeast part of China will increase constantly under the 2 °C global warming scenario, while the rate of increase in the rest of the country will slow (Sun et al. 2018).

Precipitation denotes all forms of water that reach the earth from the atmosphere. The usual forms of precipitation are rainfall, snowfall, hail, frost and dew. Of all these, the first two contribute significant amounts of water. Snowfall, as the solid precipitation, is the most important water sources in the cold season and has a significant influence on the hydrologic cycles, which also affects the water allocation, especially before the rainy season. In the text next, precipitation mentioned all refers to total precipitation. Moreover, snowfall is more sensitive to temperature change than rainfall (Ning and Bradley 2015; Pepin et al. 2015). When considering the potential for future changes in snowfall under the global warming condition, it is important to recognize that snowfall requires the coexistence of sufficiently cold temperatures and the occurrence of precipitation. In the past few decades, the snowfall exhibited a decreasing trend in the eastern China and an increasing trend in the northern Xinjiang and the eastern Tibetan Plateau (Sun et al. 2010). Changes in snowfall will be governed, therefore, by the interplay between changes in temperature and precipitation (Kunkel et al. 2007). As the main precipitation patterns in cold regions, changes in snowfall can result in some differences in water storage, and snowmelt amount in springtime (Kunkel et al. 2009). Hence, it is of interest to assess the significance of precipitation changes and snowfall changes under global warming scenarios of 1.5 °C and 2 °C, especially in the UYRB, which is the main snowfall area of the Yangtze River Basin (YRB).

The Coupled Model Intercomparison Project Phase 5 (CMIP5) has provided multi-model simulations at global scales, and such models provide a useful way to study the potential effects of future temperature and precipitation and snowfall changes (Chaturvedi et al. 2014; Ji and Kang 2013). General Circulation models (GCMs) can describe the magnitude and trends of observed global temperatures well (Wang and Chen 2013). The Fifth Assessment Report (AR5) of the IPCC reported that increases in the annual mean temperature and the frequency of heavy precipitation events have been observed in China during the past century and are very likely to increase in the future (Gemmer et al. 2010; Trenberth et al. 2007; Yang et al. 2017). The CMIP5 has provided a series of model and output data which provide many studies have analyzed and assessed temperature and precipitation in China. The results have shown that most of the models describe the temporal and spatial characteristics of the trends well over long-term time scales (Huang et al. 2013; Xu and Xu 2012). In this study, we used data from six CMIP5 models with a multi-model ensemble for three Representative Concentration Pathways (RCPs) to compare global, and regional projections in terms of the timing and magnitude of the changes in temperature, precipitation and snowfall for different global warming thresholds.

Simulated outputs (precipitation and temperature) from GCMs can exhibit large systematic biases relative to observational datasets (Lafon et al. 2013). The errors in GCM outputs can be classified as being due to (1) unrealistic large-scale variability or response to climate forcings, (2) unpredictable internal variability that differs from observations, or (3) errors in convective parameterizations and unresolved subgrid-scale orography (Eden et al. 2012). Therefore, in recent years, studies have been done to assess how best to remove the bias of GCM simulation. A range of established bias correction techniques have been evaluated to determine which is the most effective and robust method to use when correcting daily precipitation simulated by GCMs. Quantile mapping (QM) has been proven to be one of the most effective methods for bias correction for GCM precipitation and temperature (Lafon et al. 2013).

The objective of the study was to analyze the changes in precipitation and snowfall patterns over the UYRB as calculated by GCMs of CMIP5, which has been proven to be capable of reproducing the climate conditions in China with the correction by QM method. Seven precipitation and six snowfall indices were employed to assess changes in the precipitation pattern and snowfall pattern over the UYRB under 1.5 °C and 2 °C global warming scenarios, relative to the baseline period of 1986–2005. An assessment of such changes can support policy makers in the development of strategies for adapting to potential risks from climate change.

2 Materials and methods

2.1 Study area

The UYRB is located in the west highland geographical region of China, approximately 60% of which is covered by seasonal snow. The UYRB's longitude ranges from 90° E to 105° E, its latitude from 25° N to 36° N, and its elevation from 265 to 6492 m, and it covers an area of approximately 8.6×10^5 km^2 (Fig. 1). The UYRB stretches across three climate zones: the plateau climate zone (an arid area), the north subtropical zone (a semi-humid area) and the middle subtropical zone (a humid area). The vertical climate zones of the UYRB are very distinct. In the UYRB, which is influenced by warm ocean airflow and west Pacific subtropical high pressure, summer precipitation is higher than in other areas at the same latitude. In the eastern part of the basin, precipitation is abundant as a result of warm and humid currents from the Pacific Ocean and the Indian Ocean, and the annual average precipitation is typically 800–1500 mm. The amount of precipitation decreases from east to west and from south to north.

2.2 Data

Climate projections from GCMs were obtained from the World Climate Research Programme's (WCRP's) Coupled Model Intercomparison Project phase 5 (CMIP5) multi-model dataset. The data were downloaded from the website https://esgf-node.llnl.gov/search/cmip5/. The variable of temperature and precipitation and snowfall were simulated by the CMIP5 model over a historical time frame (1850–2005) and a twenty-first century time frame (2006–2100), employing three different radiative forcing scenarios. Representative Concentration Pathways (RCPs), which were designed to accommodate a wide range of possibilities in social and economic development (Moss et al. 2010). The estimated radiative forcing values by the year 2100 were 2.6 Wm^{-2} in the RCP2.6 experiment, and 4.5 Wm^{-2} and 8.5 Wm^{-2} in the other two experiments, RCP4.5 and RCP8.5 (Meehl and Bony 2011). Six models' simulations over the historical time frame and three RCPs experiments were chosen to identify the future horizons corresponding to the 1.5 °C and 2 °C global warming scenarios: Had-GEM2-ES, GFDL-ESM2-M, IPSL-CM5A-LR, MIROC-ESM-CHEM, MPI-ESM-LR, and Nor-ESM-1M, respectively (Table 1). These models have been shown to effectively simulate the climate changes in China, as a whole, and the UYRB (Chen et al. 2017; Sun et al. 2018). To account for the different spatial resolutions between the individual models and observational data, this analysis interpolated all data to a common 1° × 1° grid, which was to match the lowest resolution among these models used in this study. A multi-model ensemble, defined as the average of simulation results from multiple models, was used for the analysis (Sun et al. 2018; Chen et al. 2017).

Meteorological data for bias correction are from the Chinese Meteorological Data Sharing Network (https://data.cma.cn/), which include daily air temperature and daily precipitation data, were used. They were interpolated to a spatially and temporally continuous form based on the Gradient Plus Inverse Distance Squared (GIDS) method.
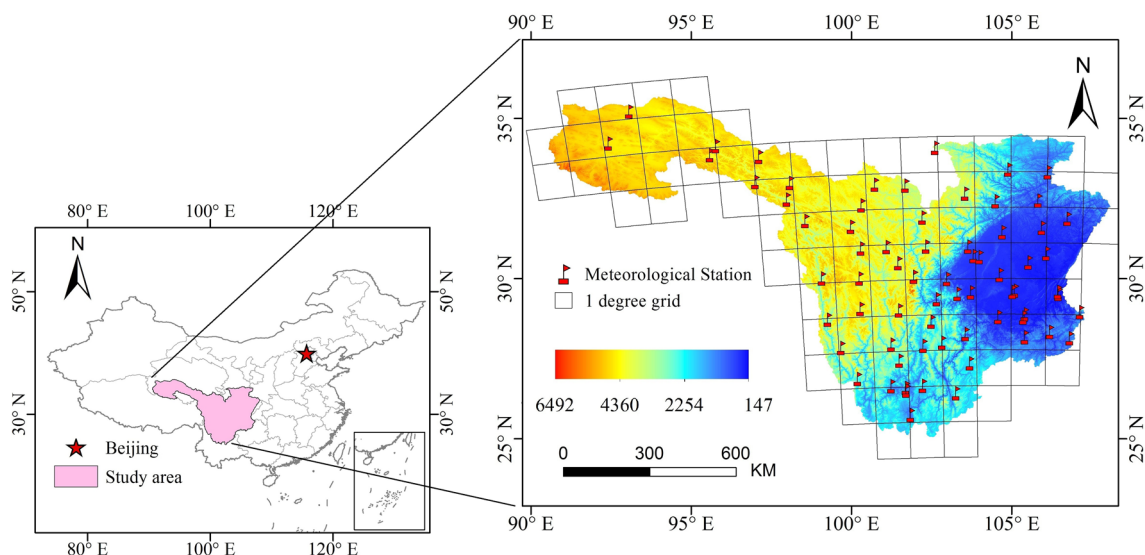

Fig. 1 The location of the study area, with the digital elevation model showing in meters

Table 1 Information about models used in this study

Model name	Institute (country)	Grids in Lon×Lat
GFDL-ESM-2M	Geophysical Fluid Dynamics Laboratory, (USA)	144×90
Had-GEM2-ES	Met Office Hadley Centre, (UK)	192×145
IPSL-CM5A-LR	Institute Pierre-Simon Laplace, (France)	96×96
MIROC-ESM-CHEN	Atmosphere and Ocean Research Institute (The University of Tokyo), National Institute for Environmental Studies, and Japan Agency for Marine-Earth Science and Technology, (Japan)	128×64
MPI-ESM-LR	Max Planck Institute for Meteorology, (German)	192×96
Nor-ESM1-ME	Norwegian Climate Centre, (Norway)	144×96

2.3 Methods

2.3.1 Bias correction of GCM outputs

Because of QM bias correction algorithms are effective at removing historical biases relative to observations, it has been proven to be artificially corrupt future model-projected trends (Cannon et al. 2015). Therefore, the QM method is used for bias correction for GCM precipitation and temperature. It is assumed that in this method, biases relative to historic observations will be constant during the projections.

QM matches the cumulative distribution function (CDF) of GCM forecasts to the CDF of observations. For ensemble forecasts, the matching takes place at the level of individual ensemble members. QM is formulated as follows (Gudmundsson et al. 2012):

$$x' = F_O^{-1}\left[F_x(x)\right] \quad (1)$$

where x and x' are raw and post processed forecasts, respectively, and $F_x()$ and $F_O()$ denote the CDFs of raw forecasts and observations. Equation (1) can also be expressed as follows:

$$F_O\left(x'\right) = F_x(x) \quad (2)$$

According to Eqs. (1) (2), a new raw forecast value is post processed in two steps. First, a quantile fraction (or cumulative probability) is determined for the raw forecast by its position in the CDF of (preceding) forecasts. Second, a new post processed value of the forecast ensemble member is generated by ''looking up'' that quantile in the CDF of the observations (Gudmundsson et al. 2012).

QM is conceptually simple and can be implemented relatively easily: $F_x()$ and $F_O()$ can be derived parametrically by fitting a distribution to the data (Gudmundsson et al. 2012) or non-parametrically using an empirical distribution function, ''lookup table,'' or kernel density estimation.

A common approach to QM is to solve Eq. (2) using the empirical CDF of observed and modeled values instead of assuming parametric distributions. The empirical CDFs are approximated using tables of the empirical percentiles. Values in between the percentiles are approximated using linear interpolation. The core of the QM method is to employ the relationship between the observed and simulated data to validate future GCM data. The QM method has been implemented in the R language and bundled in the package "qmap" which has been made available on the Comprehensive R Archive Network (https://www.cran.r-project.org/) (Gudmundsson et al. 2012).

2.3.2 The ensemble empirical mode decomposition (EMMD)

The ensemble empirical mode decomposition (EMMD) method was used in this study to analyze the long-term variation characteristics of precipitation and snowfall. The EMMD method provides an accurate analysis of a time series (Wu and Huang 2009) and is an adaptive method for representing a nonlinear and non-stationary signal as the sum of signal components with amplitude- and frequency-modulated parameters using a noise-assisted analysis technique (Huang et al. 1998) with a wide applications (Liu et al 2018). This method decomposes a time series into intrinsic mode functions (IMFs) and a residual (RES).

The IMFs are defined by the following conditions (Huang et al. 1998): (1) over their entire length, the number of extrema and the number of zero-crossings must either be equal or differ by one at most; and (2) at any point, the mean value of the signal defined by the local maxima and the envelope defined by the local minima is zero. In general, an IMF indicates a simple oscillatory mode, compared with a simple harmonic function. A time series $X(t)$ ($t = 1, 2,…., n$) can be decomposed through processes that can be briefly described as follows (Huang et al. 1998):

(1) Identify all local maxima and minima points for a given time series.

(2) Connect all local maxima points to form an upper envelope $e_{max}(t)$ and all minima points to form a lower envelope $e_{min}(t)$ using spline interpolation, respectively.

(3) Calculate the mean $a(t)$ between two envelopes.

$$a(t) = \left(e_{\max}(t) + e_{\min}(t)\right)/2 \qquad (3)$$

(4) Extract the mean from the time series and calculate the difference $h(t)$ between $X(t)$ and $a(t)$.

$$h(t) = X(t) - a(t) \qquad (4)$$

(5) If $h(t)$ meets the two conditions of IMFs according to a stopping criterion, $h(t)$ is denoted as the first IMF [written as IMF1(t) with 1 is its index]; if $h(t)$ is not an IMF, $X(t)$ is replaced with $h(t)$ and iterate steps 1–4 are repeated iteratively until $h(t)$ meets the two conditions of IMF.

(6) The residual RES1(t) = $X(t − \text{IMF1}(t))$ is then treated as new data and is subjected to the same shifting process as described above for the next IMF from RES1(t). The shifting procedure can be stopped when the residue RES(t) becomes a monotonic function or has at most has one local extreme point from which no more IMFs can be extracted (Huang et al. 2003).

At the end of this shifting procedure, the original time series $X(t)$ can be expressed as the sum of multiple IMFs and a RES:

$$X(t) = \sum_{i=1}^{n} IMF_i(t) + RES_n(t) \qquad (5)$$

where n is the number of IMFs, $RES_n(t)$ is the final residual and $IMF_i(t)$ are nearly orthogonal to each other, and all have zero means.

2.3.3 Analysis indices

Seven precipitation indices (Sun et al. 2007) and six snowfall indices were used to analyze the variation characteristics of precipitation and snowfall in the UYRB. The thirteen indices are listed in Table 2

2.3.4 Determination of future time points for 1.5 °C and 2 °C warming scenarios

The GMAT during the period from 1986 to 2005 was approximately 0.61 °C higher than during the pre-industrial for the period from 1850 to 1900 (IPCC 2013). This means that increases of another 0.89 °C and 1.39 °C in GMAT correspond to global warming of 1.5 °C and 2 °C, respectively. To analyze the change characteristics of precipitation and snowfall under different future temperature increase scenarios, the time points at which the GMAT increases to 1.5 °C and 2 °C should be calculated (Chen et al. 2017; Sun et al. 2018). Moreover, two 20-year periods around the time points of different temperature thresholds warming will be adopted as the analysis periods (Su et al. 2017). Firstly, the value of GMAT during 1988–2100 was calculated. Secondly, the increase of GMAT during 1986–2005 was calculated. Finally, the time points of 1.5 °C and 2 °C warming was found. However, one model alone has great uncertainty. Therefore, six models and their ensemble simulation were used to obtain the time points for 1.5 °C and 2 °C global warming.

3 Results

3.1 Bias correction results

The GCMs' simulated precipitation and temperature were corrected using the QM method. Figure 2 presents scatterplots of QM-based bias-corrected GCM data and raw GCM data. The corresponding standard deviations (SDs) and coefficients of determination are also presented.

As Fig. 2 shows, the accuracy of the GCMs data was improved by the QM-based bias correction. The coefficient

Table 2 Climate indices used in this study

| Index		Meaning
Total Precipitation	PA	Annual precipitation: the sum of daily precipitation in a year (mm)
	FPD	Frequency of precipitation: annual number of days of when precipitation is $0 < p$ (d)
	FTD	Frequency of trace precipitation: annual number of days when precipitation is $0 \leq p < 1$ mm (d)
	FLD	Frequency of light precipitation: annual number of days when precipitation is $1 \text{ mm} \leq p < 10$ mm (d)
	FMD	Frequency of moderate precipitation: annual number of days when precipitation is $10 \text{ mm} \leq p < 25$ mm (d)
	FHD	Frequency of heavy precipitation: annual number of days when precipitation is $25 \text{ mm} \leq p < 50$ mm (d)
	FID	Frequency of intense precipitation: annual number of days when precipitation is $p \geq 50$ mm (d)
Snowfall	FDS	First day of snowfall, snow year defined from September 1 to August 31 of next year
	LDS	Last day of snowfall
	ASF	The sum of daily snowfall in a year (mm)
	FSD	Number of snowfall days
	SI	Snowfall intensity, defined as the ratios of ASF to FSD
	MSF	Maximum of daily snowfall during the snow year
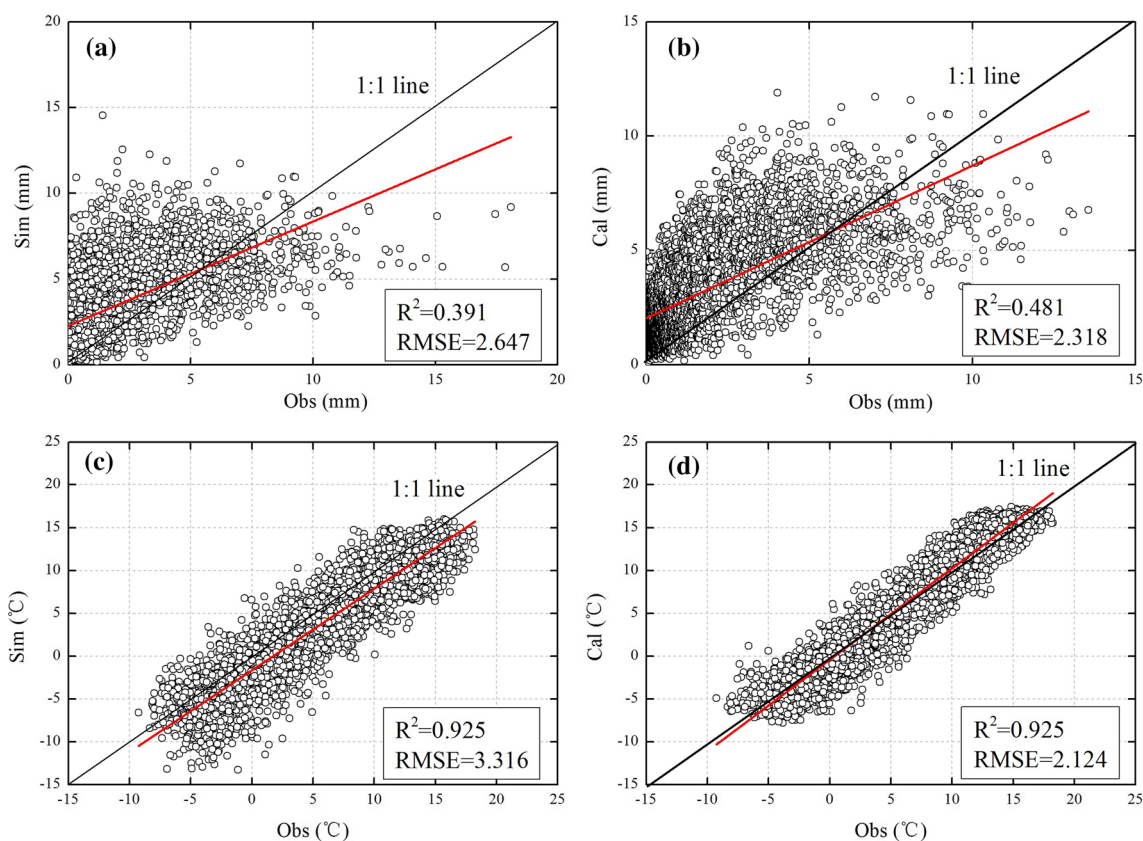
Fig. 2 Scatterplots of daily raw GCMs data (sim) and observed values (obs), and QM-based bias-corrected GCM data (cal) and observed values. **a** and **b** Are daily precipitation plots; **c** and **d** are daily temperature plots

of determination (R^2) of the GCMs simulated versus observed daily precipitation was 0.391, whereas the R^2 of the calculated versus observed daily precipitation was increased to 0.481. The R^2 of the GCMs simulated versus observed daily temperature was 0.925, and that of the calculated daily temperature was the same. However, the calculated values were closer than GCM simulation values to the observed values. The differences between the R^2 values for precipitation and temperature were mainly a result of the greater randomness of daily precipitation. In general, the QM method improved the accuracy of the GCM simulations.

3.2 Comparison between threshold crossing times for global and UYRB mean temperatures

Changes in the ensemble of multi-GCMs' GMATs for three RCPs relative to the baseline period of 1986–2005 are shown in Fig. 3.

Changes in the mean annual temperature (MAT) for the period of 2006–2100 relative to pre-industrial mean level, globally and for the UYRB, for multi-CMIP5 models under three RCPs and the historical time frame are also shown in Fig. 3. Although the global and UYRB MATs exhibit

similarly increasing trends, the rate of increase in the MAT for the UYRB is greater than the global rate of increase for all RCPs. The ensemble mean GMAT is projected to reach 1.5 °C by 2043 for RCP4.5 and by 2038 for RCP8.5, whereas the 2 °C warming target is projected to be reached by 2047 for RCP 8.5 and by 2062 for RCP4.5, and the increase in GMAT for RCP2.6 does not reach the 2 °C threshold. For the UYRB, the MAT is predicted to reach 1.5 °C by 2029 for all RCPs, and the 2 °C target is predicted to be reached by 2048 for RCP4.5 and by 2040 for RCP8.5.

Documented research shows that the increasing of temperature shows an obvious spatial variability over the UYRB, with north part's temperature being increasing faster than south part's temperature (Xu et al. 2009). To reduce the error caused by spatial variability of the time points over the basin, two 20-year periods around the years of 2031 (the average time point at which 1.5 °C warming is projected to be reached under all RCPs) and 2044 (the average time point at which 2 °C warming is projected to be reached under all RCPs) were compared to the 1986–2005 baseline period to assess the impacts of climate change on precipitation and snowfall over the UYRB under the 1.5 °C and 2 °C GMAT increase scenarios. That is, the time periods of 2025–2044
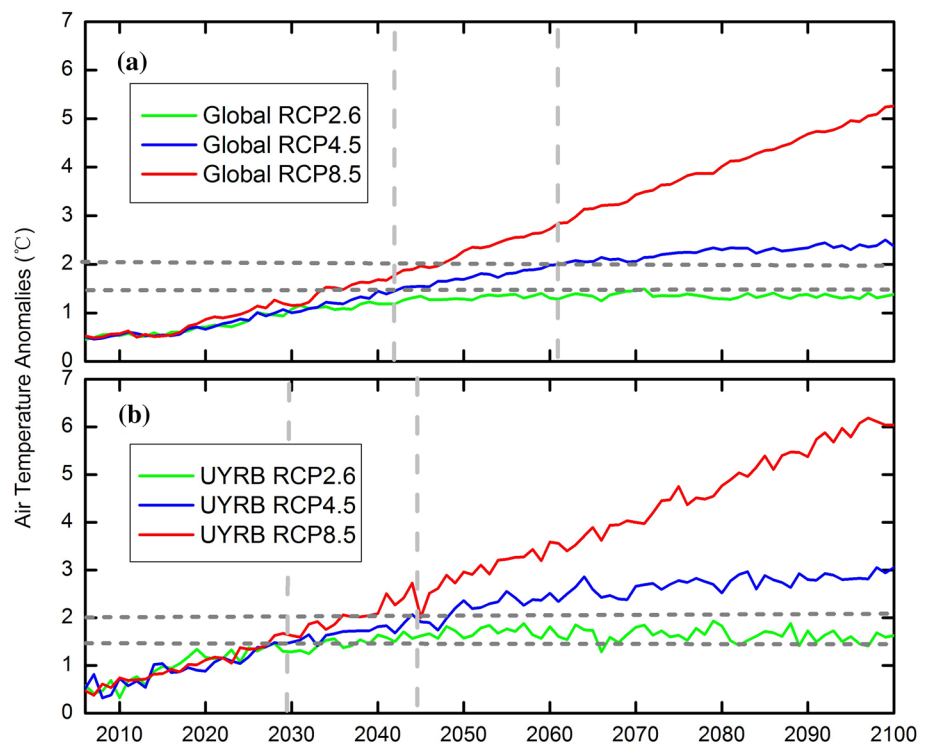
and 2036–2055 were selected for use in assessing the impact of global warming on precipitation and snowfall in the UYRB.

3.3 Variation characteristics of precipitation

3.3.1 Temporal variation of precipitation

The projected variations in precipitation globally and for the UYRB and for the three RCPs for the period of 2006–2100 are shown in Fig. 4.

As Fig. 4 shows, the predicted annual precipitation (PA) for the UYRB exhibits an overall increasing trend over the next 100 years for all of the RCPs. For RCP2.6, the PA exhibits an increasing-steady-increasing trend. For RCP4.5 and RCP8.5, PA exhibits fluctuating increasing trends. These phenomena can also be observed in the global PA predictions, which increase in almost in linear fashion.

According to the moving average of the precipitation anomaly, precipitation does not exhibit an absolutely linear change for all RCPs over the UYRB. However, precipitation on global scale for all RCPs is projected to exhibit a linear change trend in the future. The impact of the signal fluctuation frequency and amplitude in each scale of the original data can be expressed as the variation contribution rate. After decomposing the original PA series of the UYRB over the period 2006–2100 using the EEMD method, the variance contribution rate of four IMFs (IMF1–4) and one trend component RES were obtained, as shown in Table 3.

As listed in Table 3, the contribution rate of the quasi-3-year function (IMF1) reaches 29% for RCP2.6, which is the largest among all RCPs. The contribution rate of trend component (RES) is as much as 85.3% under the RCP8.5, and the PA of the UYRB exhibits an approximately linear increasing trend during the period 2006–2100. In addition, the increasing rate exhibits an upward trend from RCP2.6 to RCP8.5. The increasing of temperature can enhance the evaporation of water, which could raise the content of vapor in the air, and then increase the amount of precipitation.

The change in PA over the long time period is more strongly linear, especially for the RCP4.5 and RCP8.5 scenarios. The projected variations in PA over the UYRB under the 1.5 °C global warming and 2 °C global warming scenarios for different RCPs are shown in Fig. 5.

Figure 5 indicates that, for all RCP scenarios, PA exhibits an overall increasing trend under both 1.5 °C and 2 °C warming conditions in comparison to the baseline period, but with different change characteristics. When global warming reaches 1.5 °C during the period 2025–2044 (Fig. 5a), the increasing rate of PA under RCP4.5 is the largest. The slopes are 0.98 mm/year for RCP2.6, 4.25 mm/year for RCP4.5, and 3.14 mm/year for RCP8.5 during the period of 2025–2044. The average change magnitudes are on the order of 60 mm for RCP2.6, 46.8 mm for RCP4.5 and 38.3 mm for RCP8.5. Under the 2 °C global warming scenarios (Fig. 5b), the PA shows variations similar to those under the 1.5 °C warming condition. The slopes are 0.49, 1.18, 3.72 mm/year for RCP2.6, RCP4.5, and RCP8.5 during
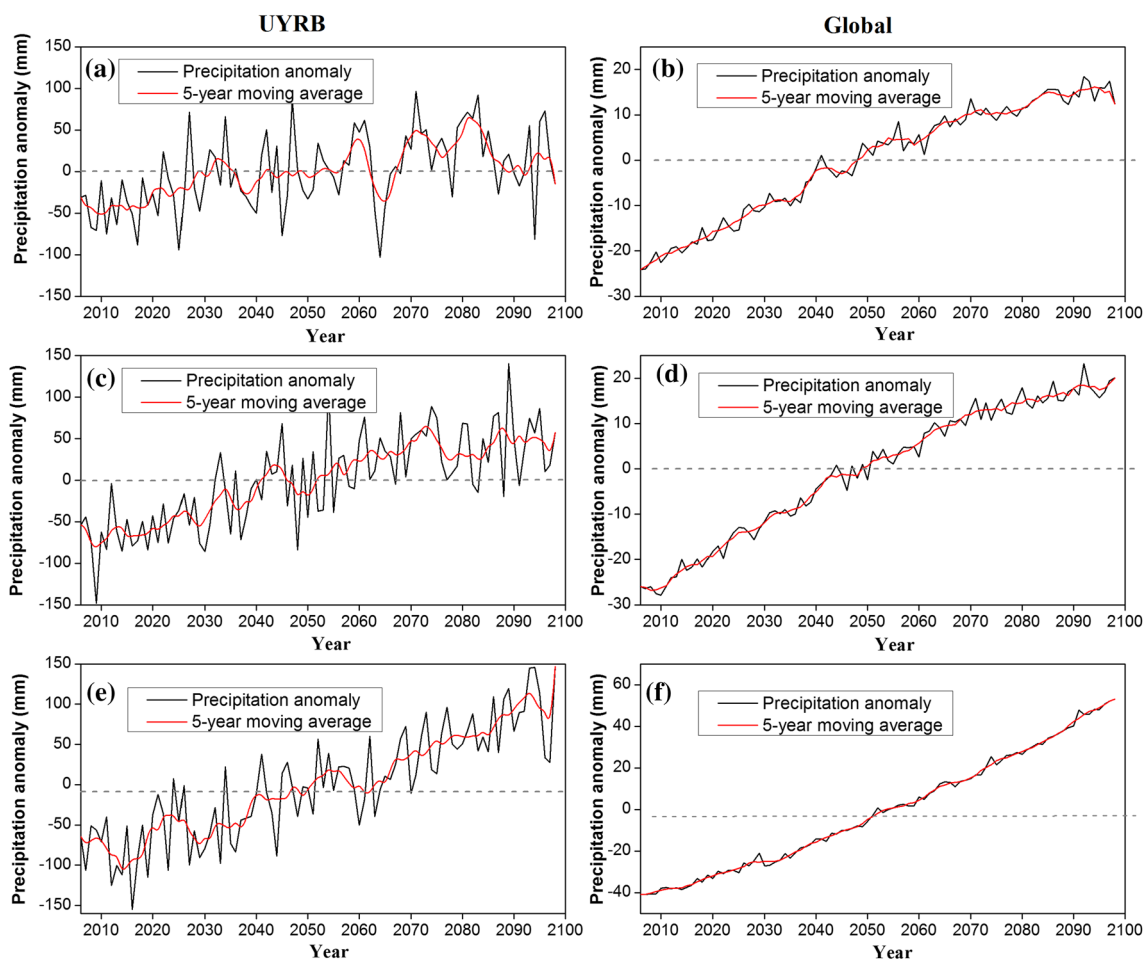
Fig. 4 Variation in annual precipitation (PA) anomaly for the period of 2006–2100 in the UYRB (left column) and globally (right column) for the three RCP scenarios. **a**, **c** and **e** Plots of PA variation over the UYRB for RCP2.6, − 4.5, and − 8.5, respectively. **b**, **d** and **f** are plots of global PA variation for RCP2.6, − 4.5 and − 8.5, respectively

Table 3 Variance contribution rates of IMFs and trend component for precipitation anomaly, based on EEMD method

|	IMF components	RCP2.6	RCP4.5	RCP8.5
Period (year)	IMF1	2.6	2.8	2.7
	IMF2	5.5	5.9	5.9
	IMF3	10.4	13.4	10.4
	IMF4	36.1	29.2	34.5
	RES	–	–	–
Contribution (%)	IMF1	29	14.3	9.8
	IMF2	7.8	2.6	2.8
	IMF3	5.6	1.8	1.6
	IMF4	1.7	1.1	0.5
	RES	55.9	80.2	85.3

the period of 2036–2055, only RCP8.5 passed the significant test with a level of $p < 0.001$. The trend of PA under different RCPs significantly, study shows that PA increased the

most under RCP4.5 compared with other two RCPs over the UYRB (Zhang 2013), which is agreed with the results of Fig. 5. The average of change magnitudes is on the order of 61.3 mm for RCP2.6, 78.5 mm for RCP4.5 and 73.3 mm for RCP8.5.

Comparison of the changes in temperature and precipitation projected by the validated ensemble six GCMs from the CMIP5 for different global warming scenarios are shown in Fig. 6.

Figure 6 shows that a warming climate with more precipitation is predicted for the UYRB for all RCP scenarios, under both 1.5 °C and 2 °C global warming scenarios. Under the 1.5 °C warming scenario, the PA is projected to increase by approximately 4.47% per 1.0 °C for RCP2.6, 4.71% per 1.0 °C for RCP4.5, and 4.83% per 1.0 °C for RCP8.5. Under the 2 °C warming scenario, the PA is projected to increase by approximately 11.71% per 1.0 °C for RCP2.6, 9.06% per 1.0 °C for RCP4.5, and 12.54% per 1.0 °C for RCP8.5. Relative to the baseline period, the projected changes in

Fig. 5 Changes in PA of the UYRB during the period 2025–2044 for 1.5 °C global warming (**a**) and the period 2036–2055 for 2 °C global warming (**b**) relative to the baseline period 1986–2005 under RCP2.6, RCP4.5, and RCP8.5
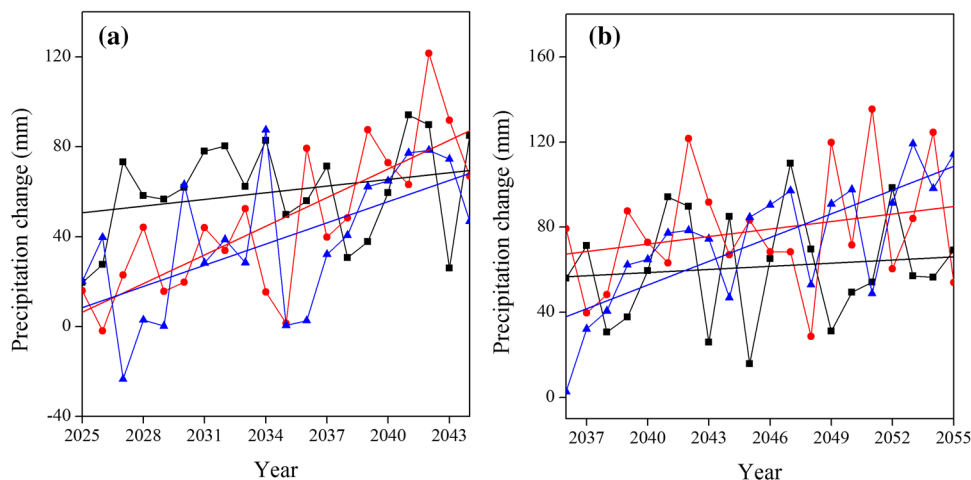
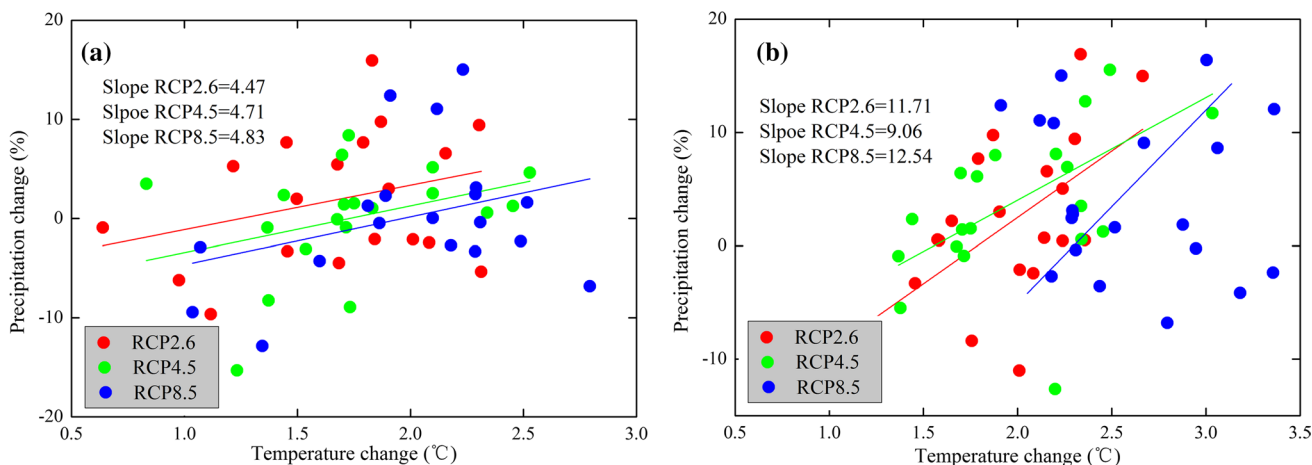|			Significance level	Slope (mm/a)
	1.5 °C global warming	RCP2.6	<0.1	0.98
		RCP4.5	<0.001	4.25
		RCP8.5	<0.01	3.14
	2 °C global warming	RCP2.6	<0.01	0.49
		RCP4.5	<0.01	1.18
		RCP8.5	<0.001	3.72

Fig. 6 Changes in MAT and precipitation of the UYRB under 1.5 °C (**a**) and 2 °C (**b**) warming scenarios for three RCP scenarios relative to the baseline period (1986–2005)

precipitation under the 2 °C warming scenario are more significant than those under the 1.5 °C warming scenario.

3.3.2 Spatial variation of precipitation

The spatial distributions of the projected amplitudes of change in PA in the UYRB for the three RCP scenarios, relative to the baseline period (1986–2005), under the 1.5 °C and 2 °C global warming scenarios are shown in Fig. 7. The significance level of all scenarios was also calculated.

Figure 7 indicates that the projected increases in PA vary with the RCP scenarios considered and exhibit

obviously spatial differences, and that most area passed $p < 0.1$ significance test. Under both the 1.5 °C and 2.0 °C global warming scenario, the PA shows an increase relative to the baseline period of 1986–2005 in more than half of the UYRB (in the most of north half of the basin), while a few parts of the UYRB (in the southern half of the basin) show a decrease. The positive change (up to 24%) is greater than the negative change (up to 12%), resulting in an average positive change in PA over the whole of the area. The positive change in the PA is lower under the 1.5 °C than under the 2.0 °C scenario for all the RCPs. However, the negative change in the PA under the
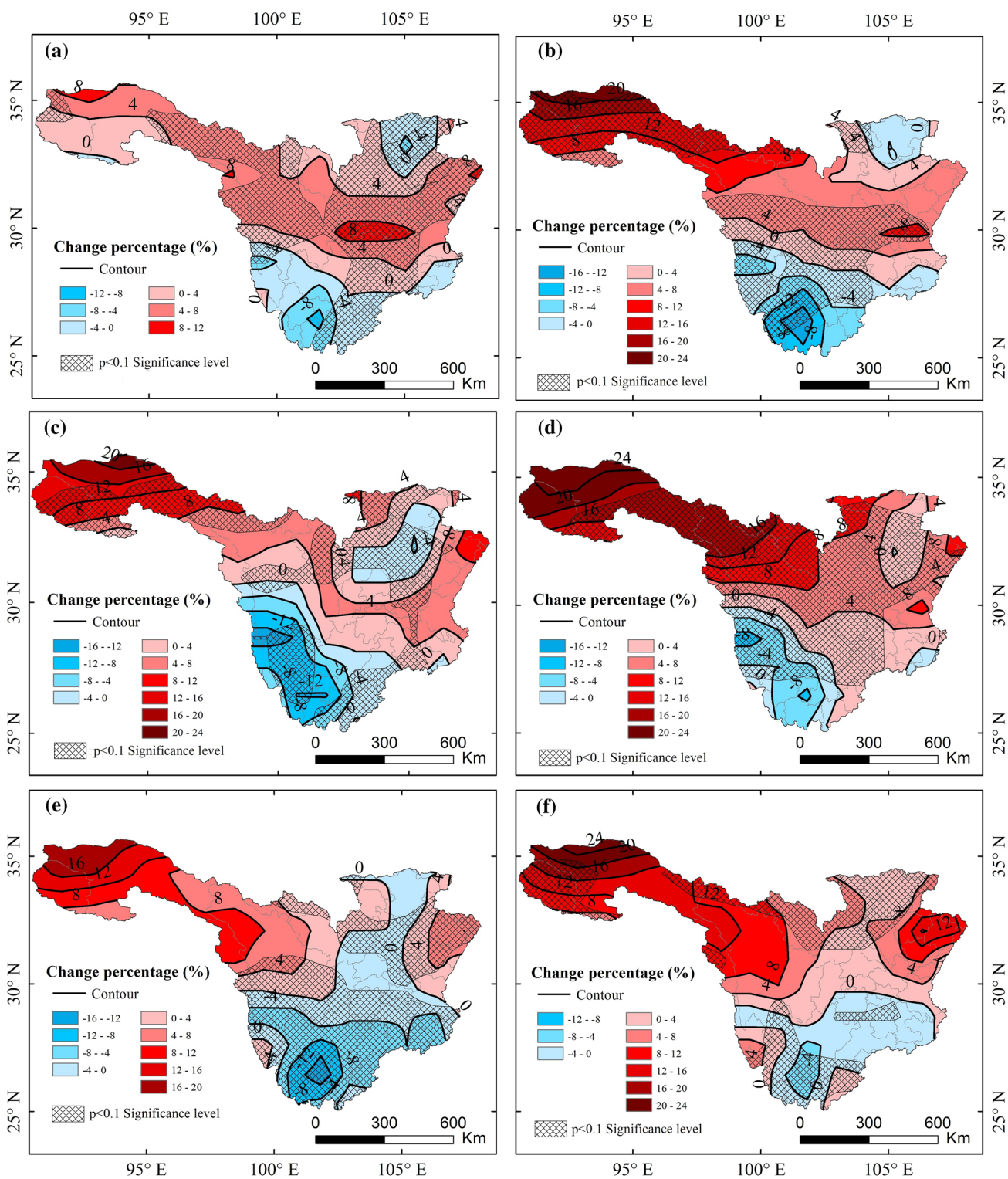
Fig. 7 Percentage changes in PA in the UYRB under 1.5 °C (left column) and 2 °C (right column) global warming scenarios corresponding to RCP 2.6 (upper panel), RCP4.5 (middle panel) and RCP8.5 (lower panel), relative to the baseline period

1.5 °C scenario is higher than that under the 2.0 °C scenario. Among all the RCPs, the PA is projected to exhibit a more obviously positive change (reaching 24%) in the

north part of the UYRB for the RCP4.5 scenario than for the other two RCPs, while a more significant negative change is (reaching 16%) in the south and east part

of UYRB for RCP 8.5 under both the 1.5 °C and 2.0 °C global warming scenarios. In general, the change in PA response to the global warming shows spatial characteristics. Precipitation increases with rising temperature, but after the temperature has risen to a certain extent, the rising trend begins to slow.

Figure 7 also shows that PA in most part of the UYRB increases with the increasing of temperature. However, over some parts of UYRB, total precipitation decrease instead. Prominently, global warming leads to stronger South Asian Monsoon and East Asian Monsoon, leading higher precipitation across China as a whole (Chen et al. 2013; O'Gorman 2014). The stronger South Asian Monsoon increased the amount of vapor transported to the UYRB, which resulted in the increasing of precipitation in the north and middle part of the UYRB (Xu and Qian 2005). This is especially true for the north and west area of the UYRB where the ratio of snowfall to total precipitation is higher than other parts. For the southeast part of UYRB, total precipitation is more complicate, the response of total precipitation to the increase of temperature is not linear. The ratio of snowfall and total precipitation is showed as Fig. 8. Different spatial patterns of precipitation change under different climate scenarios were not only caused by temperature increase but also by other climate factors, such as air pressure, relative humidity, wind speed, etc.

3.3.3 Variation in precipitation indices

The frequencies of different precipitation types for the three RCPs under the 1.5 °C and 2 °C global warming scenarios are compared with those for the baseline period of 1986–2005 in Fig. 9. The significance of changes in frequencies of different precipitation types were also calculated, which are showed in Table 4.

Table 4 shows that the change of the frequencies of different types of precipitation are not too significant under different climate scenarios, this is mainly because of that the values of frequencies of different types of precipitation show greatly randomness. It also indicates that the changes of the frequency of heavy precipitation for RCP4.5 and RCP8.5 and the frequency of intense precipitation for RCP8.5 under the 1.5 warming scenario were significant at the level of 0.1. Therefore, to overcome the randomness, shown as in Fig. 9, only the average values of different types of precipitation were analyzed.

For the baseline period of 1986–2005, the multi-year average the FPD is projected to be approximately 225, based on a multi-year average, while FTD, FLD, FMD, FHD, and FID are projected to be approximately 77, 117, 28, 4, and 0.4 on average, respectively. Under the 1.5 °C global warming scenario, although the FHD and FID increase by approximately 0.5 and 0.1 on average for RCP2.6, the FTD, FLD, and FMD decrease. For RCP4.5, only the FTD decreases, by

Fig. 8 The spatial distribution of the ratio of snowfall and total precipitation
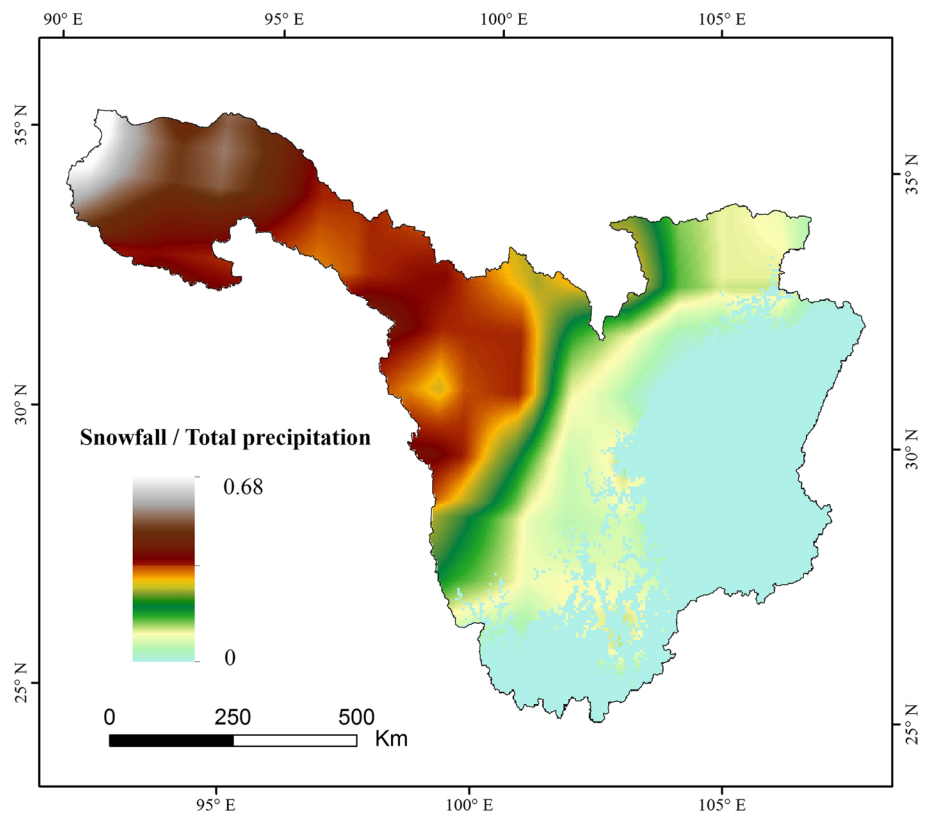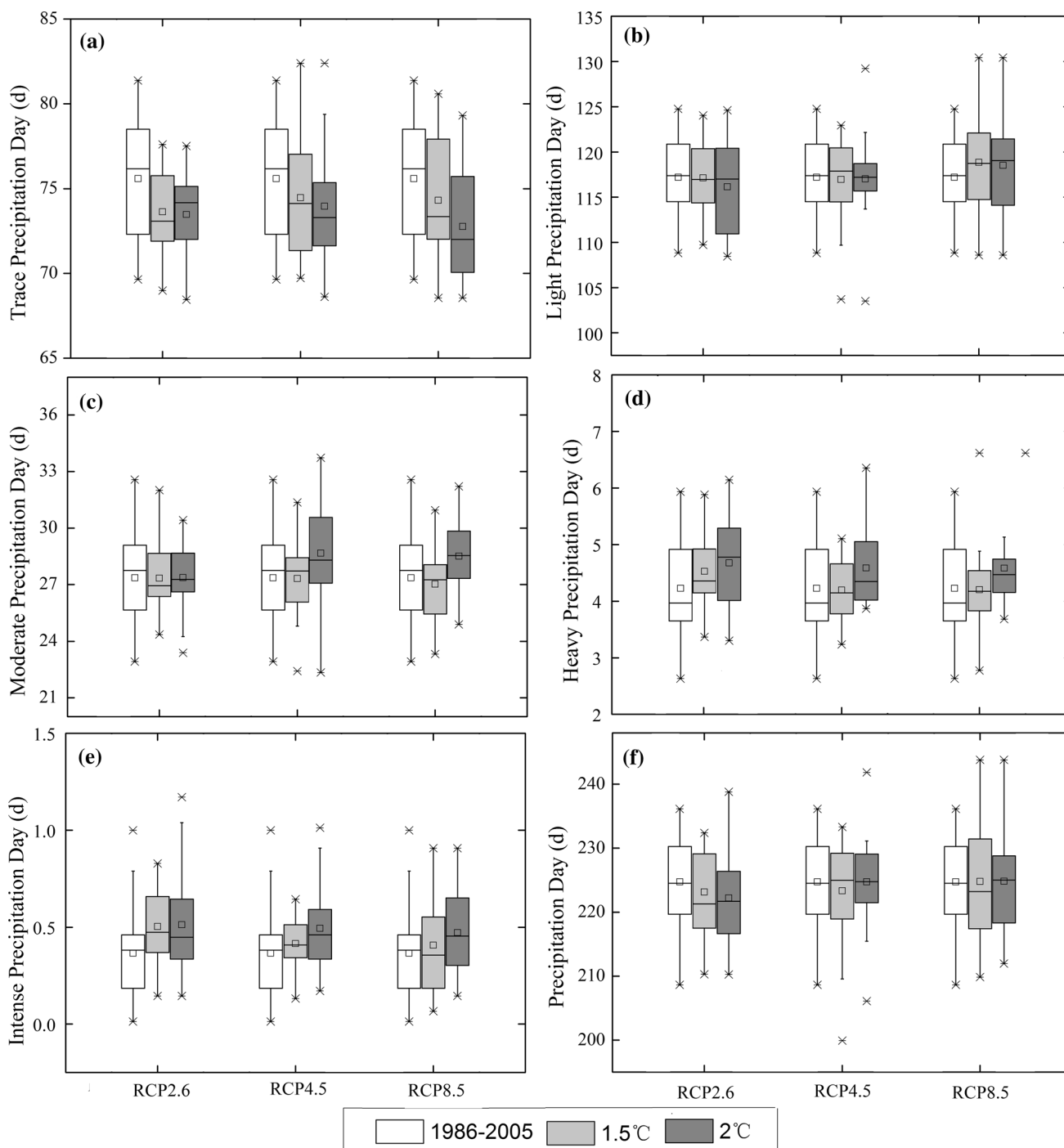
Fig. 9 Changes in precipitation days under 1.5 °C and 2 °C global warming scenarios for three RCPs as well as in the baseline period (1986–2005). The cross symbols represent the maximum and minimum values during the period. The upper edge represents the 75th percentile, the lower edge represents the 25th percentile and the middle line represents the 50th percentile. The small square represents the mean value

approximately 3; the numbers of days of other types of precipitation do not exhibit significant differences. The FTD for RCP8.5 decreases by approximately 5, while the FLD, FMD, FHD, and FID increase by approximately 4, 1, 0.5, and 0.1 on average, respectively, relative to the baseline period.

Under the 2 °C global warming scenario, the FTD and FMD decrease by 3 and 1 on average, respectively for RCP2.6; only the FHD increases, by 1. For RCP4.5, only the FTD exhibits a decreasing trend, with an amplitude of 4 days on average, while the FMD, FHD, and FID increase

Table 4 The significance level of the change in precipitation

Precipitation type	RCPs	1986–2005	1.5 °C warming scenario	2 °C warming scenario
Trace precipitation	− 2.6	0.248	0.82	0.253
	− 4.5		0.85	0.516
	− 8.5		0.608	0.776
Light precipitation	− 2.6	0.558	0.989	0.194
	− 4.5		0.906	0.832
	− 8.5		0.701	0.909
Moderate precipitation	− 2.6	0.458	0.486	0.986
	− 4.5		0.873	0.045
	− 8.5		0.255	0.651
Heavy precipitation	− 2.6	0.029	0.654	0.961
	− 4.5		0.042	0.137
	− 8.5		0.002	0.891
Intense precipitation	− 2.6	0.144	0.461	0.448
	− 4.5		0.840	0.088
	− 8.5		0.039	0.621
Precipitation day	− 2.6	0.773	0.718	0.208
	− 4.5		0.982	0.465
	− 8.5		0.957	0.932

The lower of the values, the higher of the significance of the change

by 1, 0.3, and 0.1, respectively. The FPD are not projected to change significantly relative to the baseline. For the RCP8.5 scenario, the FTD is projected to exhibit a decreasing trend of approximately 5 days on average, although the days of other types of precipitation are all projected to increase, by 2, 1.5, 0.5, 0.1 on average for light, moderate, heavy, and intense precipitation, respectively. In summary, the FTD is projected to increase for all RCPs under both the 1.5 °C and 2 °C global warming scenarios, while the frequencies of other intensities of precipitation are projected to exhibit differences for different climate scenarios.

3.4 Variation characteristics of snowfall

3.4.1 Temporal variation of snowfall

Annual snowfall (ASF) anomalies for the UYRB and globally for three RCPs for the period of 2006–2100 are shown in Fig. 10.

As Fig. 10 shows, ASF is projected to exhibit an overall decreasing trend over the period of 2006–2100 for the three RCP scenarios, both globally and for the UYRB. The global projection in particular is for more significantly decreasing trends in ASF, with the most rapidly decreasing rate in ASF projected to occur under the RCP8.5 scenario. For the UYRB, ASF is projected to exhibit a decreasing-steady-increasing trend under RCP2.6 and a relatively

stronger nonlinear trend than for the other scenarios. ASF is projected to decline throughout the whole period for the RCP4.5 scenario, with the rate of decrease after 2042 being projected to be lower than that before. The rate of decrease for the RCP8.5 scenario is projected to be larger than that for the other RCPs. The variation characteristics in the global ASF are projected to be similar to that for the UYRB but to decrease more significantly. The decreasing trend in the change in global snowfall for RCP8.5 is projected to be close to linear. The projected trend in ASF change is the opposite of that of precipitation on both the global and UYRB scales, mainly because of the projected increases in temperature. As GMAT increases, more surface water is evaporated into the atmosphere and more precipitation occurs, but this is not true for snowfall; increasing temperatures cause more liquid precipitation, which reduces the amount of solid precipitation.

The EEMD method was used to study the variation characteristics in ASF over a long period of time. After decomposing the original ASF series of the UYRB over the period of 2006–2100 using the EEMD method, four IMFs (IMF1–4) and one trend component RES were obtained, as shown in Table 5.

The results obtained for the contribution rates for the IMFs and the trend component of ASF for the UYRB exhibit characteristics similar to those for precipitation. The contribution rate of the quasi-3-year function (IMF1) is 44% for the RCP2.6 scenario, which is the largest of these rates. The contribution rate of the trend component reaches 95.4% under RCP8.5, which means that the ASF is projected to exhibit a linearly decreasing trend during the period of 2006–2100. As the RCP value increases, the decreasing trend becomes more strongly linear. This also indicates that increasing temperatures will have a significant influence in decreasing precipitation and that the rate of decrease rate will exhibit an upward trend from RCP2.6 to RCP8.5.

The projected variations in ASF in the UYRB under the 1.5 °C and 2 °C global warming scenarios for the different RCPs considered are shown in Fig. 11.

The results suggest that in the UYRB, ASF for all RCPs will exhibit a significant overall decreasing trend, especially under the 1.5 °C warming scenario. ASF is projected to decrease under the 1.5 °C global warming scenario, relative to the baseline period, for all of the RCP scenarios considered. The rates of decrease are 0.6 mm/year for RCP2.6, 1.23 mm/year for RCP4.5, and 1.35 mm/year for RCP8.5. All RCPs passed the $p < 0.05$ significance test. The multi-year average decrease is 28.3 mm for RCP2.6, 33.2 mm for RCP4.5, and 44 mm for RCP8.5 over the period of 2025–2044. The ASF in the UYRB under the 2 °C global warming scenario is projected to decrease less significantly than under the 1.5 °C global warming scenario, relative to the 1.5 °C global warming scenario. The rates of decrease
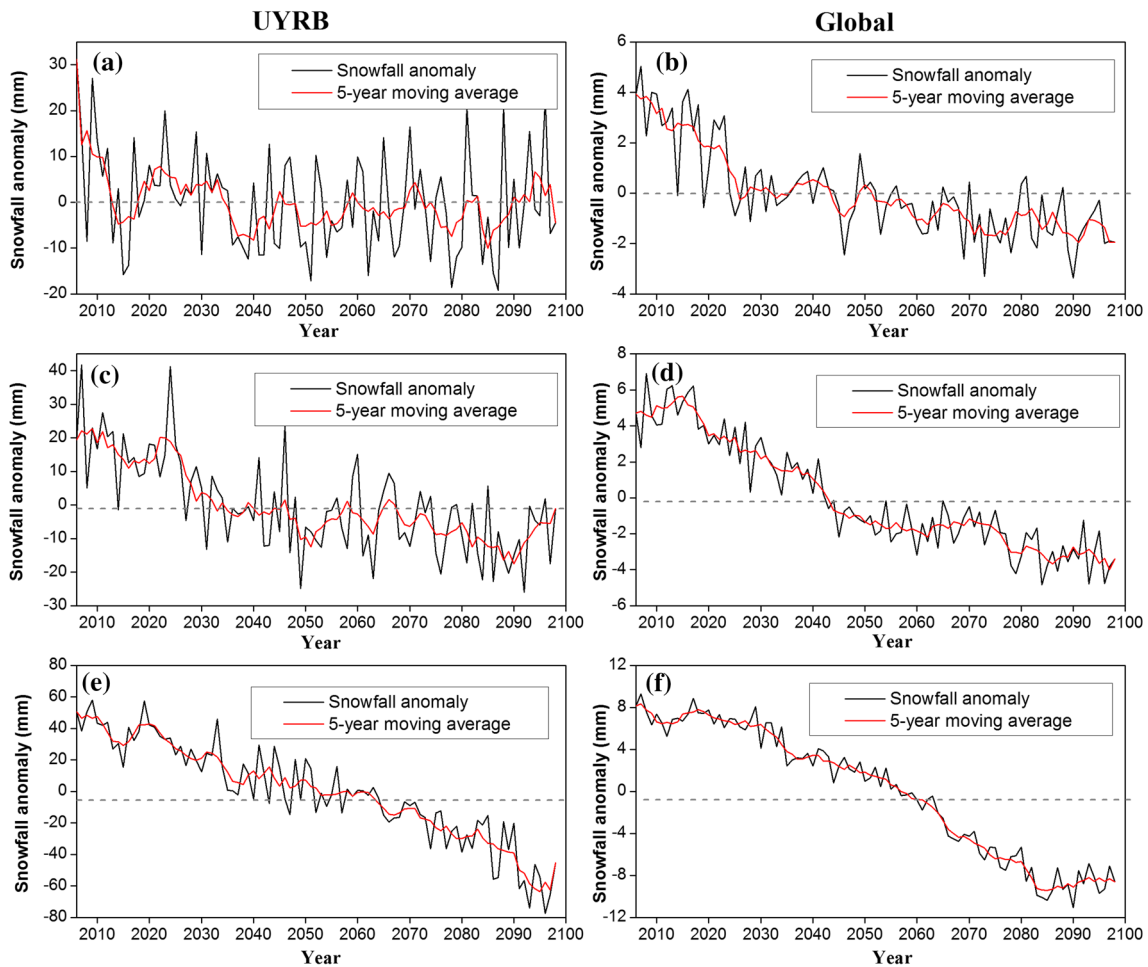
Fig. 10 Variation in annual snowfall (ASF) anomaly for the period of 2006–2100 in the UYRB (left column) and globally (right column) for scenario RCP2.6 (Top panel), RCP4.5 (middle panel) and RCP8.5 (lower panel), respectively

Table 5 Variance contribution rates of IMFs and trend component for snowfall anomaly based on EEMD method

|	IMF components	RCP2.6	RCP4.5	RCP8.5
Period (year)	IMF1	2.8	2.8	2.6
	IMF2	5.9	5.9	6.3
	IMF3	10.4	13.4	13.4
	IMF4	30	29.2	46.8
	RES	–	–	–
Contribution (%)	IMF1	44	24.4	2.1
	IMF2	15.4	5.9	0.6
	IMF3	3.6	3.7	0.4
	IMF4	5.6	1.2	1.5
	RES	31.4	64.8	95.4

are 0.13 mm/year for RCP2.6, 0.31 mm/year for RCP4.5, and 0.79 mm/year for RCP8.5, and only RCP8.5 passed the $p < 0.05$ significance test. The multi-year average decreases are 33.7 mm for RCP2.6, 39.8 mm for RCP4.5, and 55.2 mm

for RCP8.5. The projected ASF decreased the most under RCP8.5, which is mainly because of the increasing of temperature promotes the snowfall temperature threshold and leads to more liquid precipitation.

Comparisons of the changes in temperature and snowfall projected by the ensemble of six GCMs from the CMIP5 for different levels of global warming are shown in Fig. 12.

Figure 12 shows that a warming climate with less snowfall is predicted for the UYRB for all RCP scenarios under both 1.5 °C and 2 °C global warming scenario. Under the 1.5 °C warming scenario, the ASF is projected to decrease by approximately 2.6% per 1.0 °C for RCP2.6, 6.05% per 1.0 °C for RCP4.5, and 8.15% per 1.0 °C for RCP8.5. Under the 2 °C warming scenario, the ASF is projected to decrease by approximately 2.15% per 1.0 °C for RCP2.6, 2.64% per 1.0 °C for RCP4.5, and 4.36% per 1.0 °C for RCP8.5. Relative to the baseline period, the projected changes in snowfall under the 1.5 °C warming scenario are more obvious than those in the 2 °C warming scenario, which is the opposite of the changes in PA.

Fig. 11 Changes in ASF for the UYRB during the period of 2025–2044 for 1.5 °C global warming (**a**) and the period of 2036–2055 for 2 °C global warming (**b**) under RCP2.6, RCP4.5, and RCP8.5
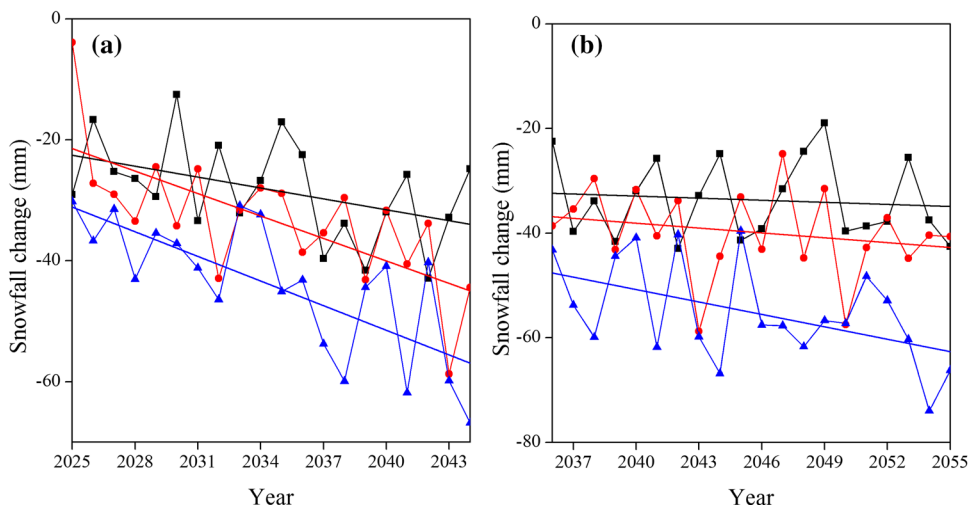
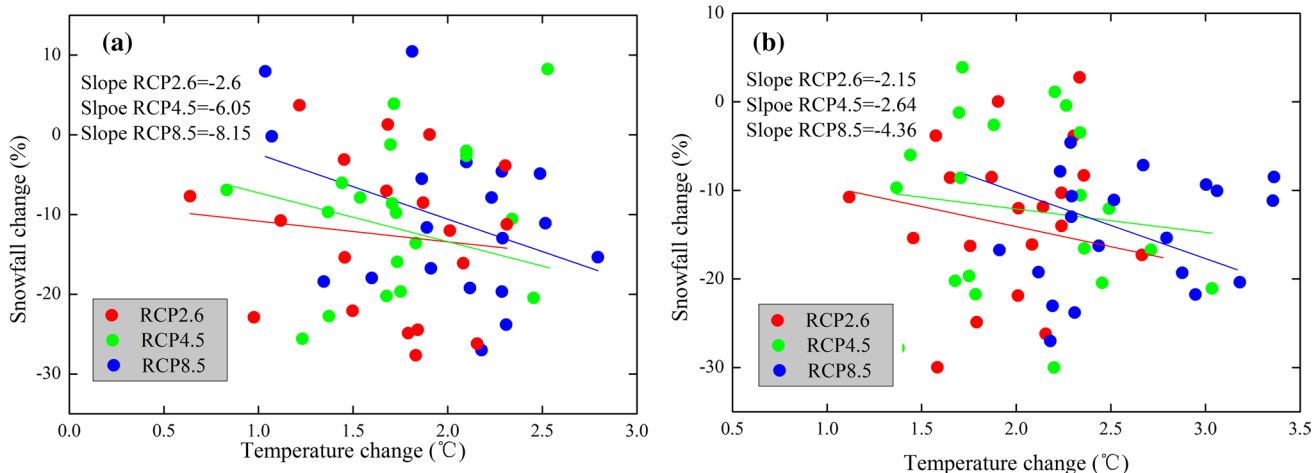|		Significance level	Slope (mm/a)
1.5 °C global warming	RCP2.6	<0.05	-0.6
	RCP4.5	<0.001	-1.23
	RCP8.5	<0.001	-1.35
2 °C global warming	RCP2.6	<0.1	-0.13
	RCP4.5	<0.1	-0.31
	RCP8.5	<0.05	-0.79

Fig. 12 Changes in MAT and snowfall in the UYRB under 1.5 °C (**a**) and 2 °C (**b**) warming scenarios for three RCP scenarios relative to the baseline period (1986–2005)

3.4.2 Spatial variation in snowfall

Spatial distributions of changes in ASF in the UYRB for the three RCP scenarios relative to the baseline period (1986–2005) under 1.5 °C and 2 °C warming scenarios are shown in Fig. 13, the significance level of every scenario was also calculated.

Figure 13 indicates that the projected decreases in ASF vary with the RCP scenario considered and exhibit spatial variation, which more than half of the UYRB passed the

$p < 0.1$ significance test, especially in the middle mountainous regions. Under both the 1.5 °C and 2 °C global warming scenario the ASF, relative to the baseline period of 1986–2005, in the most of the UYRB shows the trend of the decrease, and only few parts of the UYRB (in the north end of the basin) shows the trend of the increase. The positive change (up to 12%) is lower than the negative change (up to 60%), resulting the average change of ASF over the whole of the area is negative. The negative change of ASF under 1.5 °C global warming scenario is lower than that of under
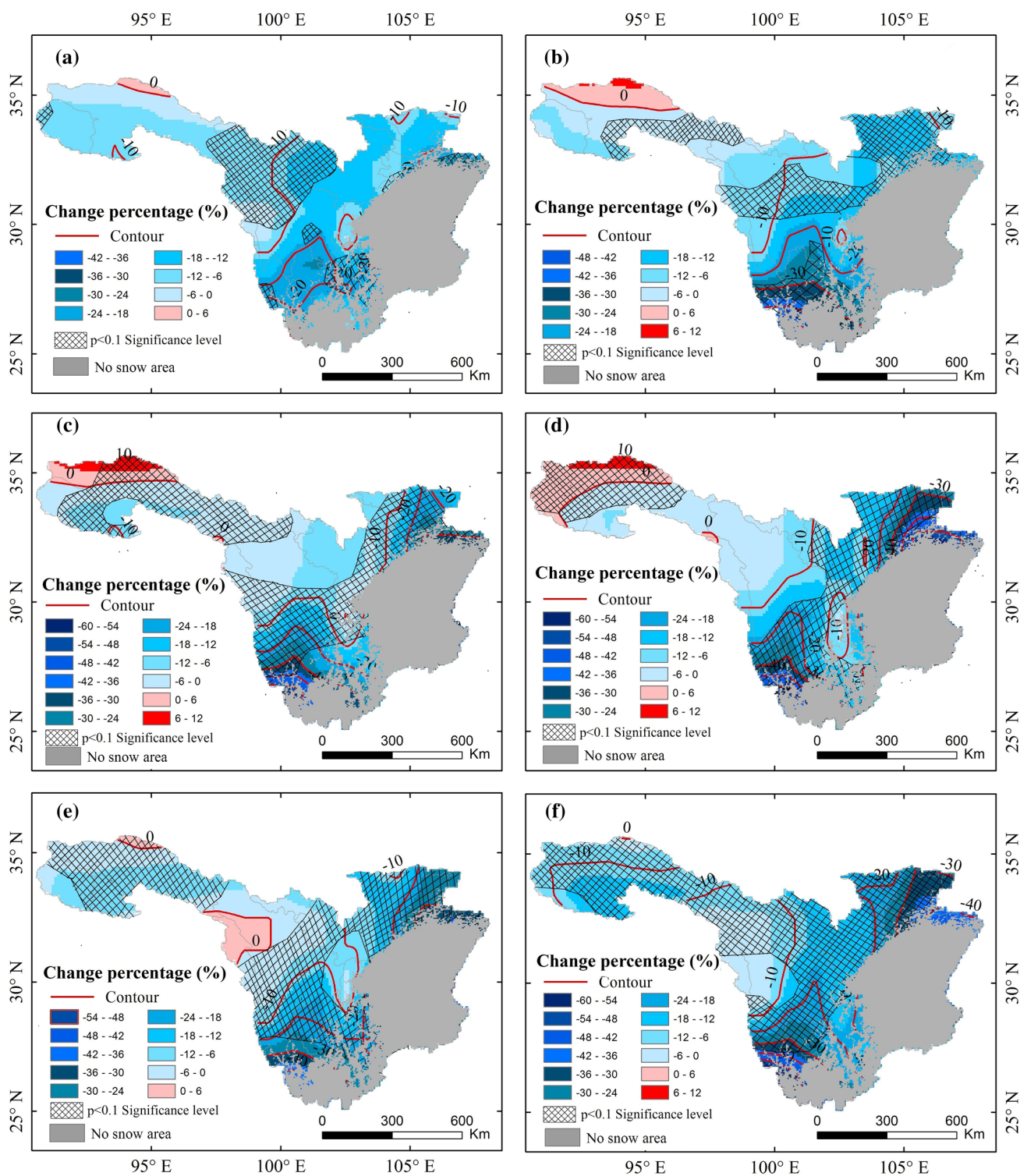
Fig. 13 Projected percentage change in ASF under 1.5 °C (left column) and 2 °C (right column) global warming scenarios in the UYRB. **a**, **c**, **e** are RCP2.6, 4.5 and 8.5, respectively. **b**, **d**, **f** are RCP2.6, 4.5 and 8.5, respectively

2 °C global warming scenario. But the positive change of ASF is higher under 1.5 °C than under 2 °C. Among all the RCPs, it is seen that the ASF is projected to exhibit a more

negative change for the RCP8.5 scenario, than that for the other two RCPs for both 1.5 °C and 2.0 °C global warming scenarios.

Snowfall mainly occurs in the northern and middle part of the UYRB with low temperature and high elevation. There is a little snowfall in the southern and eastern parts of the UYRB because of the high temperature and low elevation. Previous research found that snowfall decreased with the increase of temperature in the east of Tibetan Plateau, and that it will continue to decrease with the raising of temperature (Deng et al. 2017). Raising temperature increases the amount of available moisture in the air, but in general, also leads to a higher change of precipitation falling as rain and not snow. Thus, the snowfall will decrease in the mainly snow zone in the north and middle of the UYRB.

It is seen that the ASF is projected to exhibit a more negative change for the RCP8.5 scenario, than that for the other two RCPs for both 1.5 °C and 2.0 °C global warming scenarios. The most decrease for RCP4.5 and RCP8.5 is in the south part of the UYRB, which is almost no snowfall all the year round, and the values of the change amplitude in these areas have no significance. While, in the middle and north part of the UYRB, the decrease trend under RCP8.5 is higher than that for RCP4.5. The no-snow-area was showed in the Fig. 13. The multi-year snow area was simulated by a hydrological process-based now depth mode (Ren and Liu 2019)

3.4.3 Variation in snowfall indices

The six snowfall indices for the three RCPs under the 1.5 °C and 2 °C global warming scenarios are compared with the baseline period of 1986–2005 in Fig. 14. The significance of changes in snowfall indices are showed in Table 6.

Table 6 indicates that the first day of snowfall under 2 °C warming scenario for RCP 8.5, days of snowfall for RCP8.5 under 1.5 °C warming scenario and snowfall intensity for RCP8.5 under 1.5 °C warming scenario are significant at the level of 0.1. The annual snowfall for RCP8.5 under 2 °C warming scenario is significant at the level of 0.01. The change of most indices of snowfall are not too significant under different climate scenarios, this is mainly because of the randomness of different indices of snowfall. To overcome the randomness, only the average values of different indices of snowfall were analyzed. For the period of 1986–2005, the first snowfall in the UYRB occurred on October 17, on average, and the last snowfall occurred on July 16. ASF was approximately 240 mm per year, on average, and FSD, SI, and MSF are 102 days, 2.35 mm per day, and 36 mm, respectively. Under the 1.5 °C warming scenario, the FDS is projected to be slightly earlier than for the baseline period for RCP2.6, and delays of approximately 3 and 2 days are projected for RCP4.5 and RCP8.5, while the LDS is projected to be later for all of the RCPs, with the largest value being 11 days for RCP4.5. The ASF for

all RCPs is projected to decrease by the same amount of approximately 215 mm on average. The decrease in the FSD is not projected to exhibit obvious differences between the different RCPs, relative to the baseline period. The change in SI is projected to be larger for RCP2.6 than for the other scenarios, with an average value of approximately 2.25 mm per day. The MSF is projected to exhibit a decreasing trend, relative to the baseline period, with the largest decrease of 5 mm occurring under the RCP8.5 scenario.

Under the 2 °C warming scenario, the FDS is projected to be delayed for approximately 2, 2, and 5 days for RCPs 2.6, 4.5, and 8.5, respectively, and the LDS is projected to advance more obviously, relative to the baseline period, with the largest advance being 14 days for RCP8.5. The multi-year average of ASF for RCP8.5 is projected to decrease the most, by approximately 35 mm. The FSD is not projected to exhibit differences from that projected for the 1.5 °C warming scenario for RCP2.6, whereas for RCP8.5, the FSD is projected to decrease by approximately 17 days in comparison with the baseline period of 1986–2005. However, the SI is projected to change little, relative to the baseline period, for all of the RCPs. The MSF is not predicted to exhibit obviously change but is predicted to vary with the range of this value. For all of the scenarios, the ASF and FSD are the two indices that are projected to be most easily influenced by the warming climate, because they vary more than the other indices. Snowfall can be influenced by climate change, but this influence will be reduced when climate change reaches a threshold.

4 Summary and conclusions

Global warming has influenced the hydrological cycles in the UYRB during the twentieth century, and continued warming may have further impacts on precipitation and snowfall patterns in this region. The CMIP5 provides multi-model simulations on global scales, and such models provide a useful way to study predicted future precipitation and snowfall changes (Chaturvedi et al. 2014; Ji and Kang 2013; Mankin and Diffenbaugh 2015). However, the bias in GCMs can be the primary source of uncertainty in the assessment of climate change (Gao et al. 2019). Therefore, the QM correction method was employed to remove the bias in GCMs in this study. The change characteristics in precipitation and snowfall patterns in the UYRB under the 1.5 °C and 2 °C global warming scenarios were then evaluated.

The MAT in the UYRB is increasing more rapidly than the GMAT, and this analysis shows that the GMAT will increase 1.5 °C relative to the baseline period (1986–2005) by the year of 2034, and 2 °C by the year of 2046.
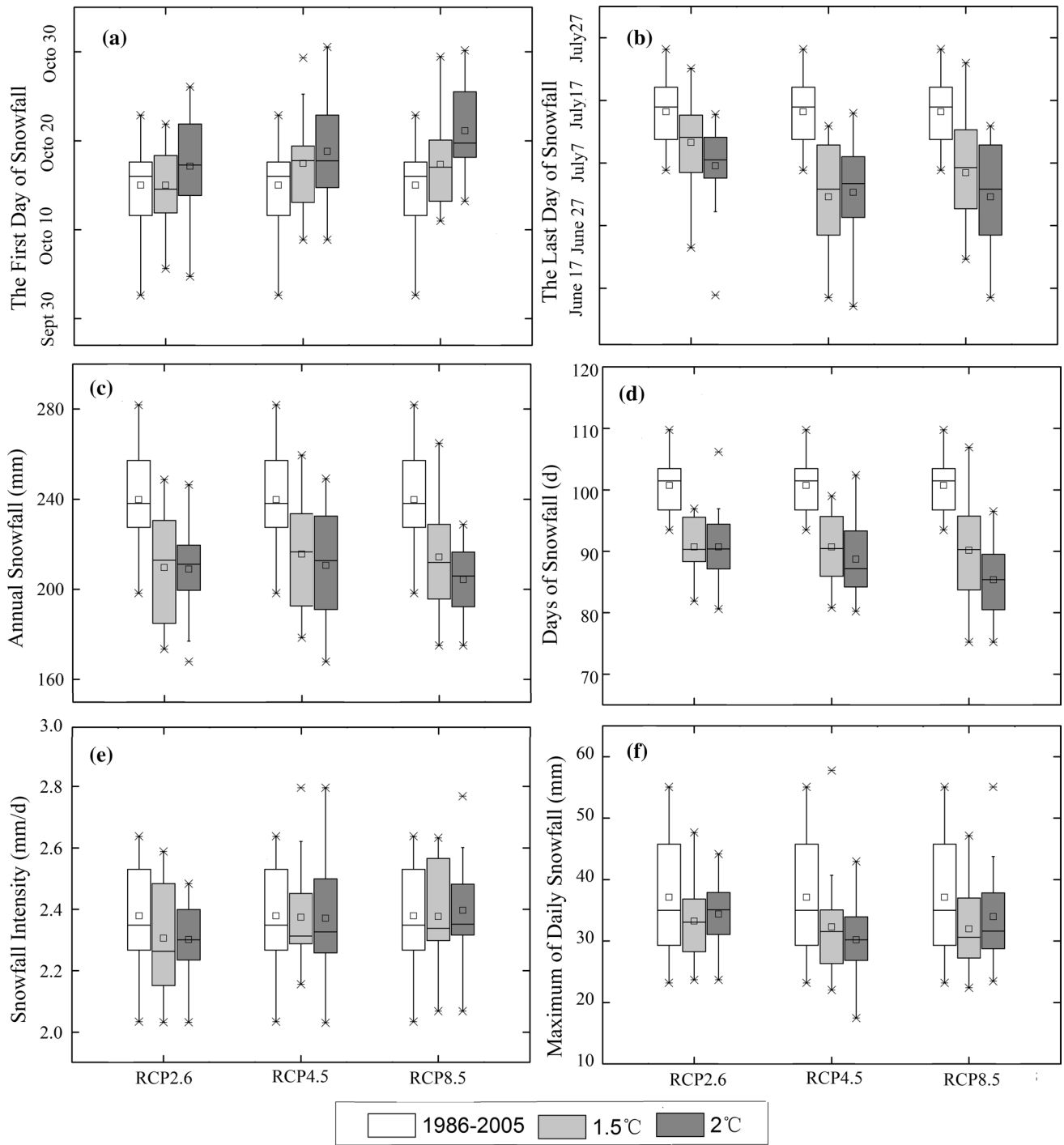
Fig. 14 Changes in snowfall indices under 1.5 °C and 2 °C global warming scenarios for three RCPs as well as in the baseline period (1986–2005). The cross symbols represent the maximum and minimum values during the period. The upper edge represents the 75th percentile, the lower edge represents the 25th percentile and the middle line represents the 50th percentile. The small square represents the mean value

The PA of the UYRB exhibits an overall increase trend with the increase of temperature (Held and Soden 2006; Sun et al. 2007; Trenberth et al. 2003). The rates of increase are 0.98 mm/year for RCP2.6, 4.25 mm/year for RCP4.5, and 3.14 mm/year for RCP8.5 under the 1.5 °C global warming scenario, which changes to 0.49, 1.18 and 3.72 mm/year under the 2 °C global warming scenario. The PA will increase by approximately 4.47%, 4.71% and 4.83% per

Table 6 The significance level of the change in snowfall

Precipitation type	RCPs	1986–2005	1.5 °C warming scenario	2 °C warming scenario
The first day of snowfall	− 2.6	0.109	0.36	0.516
	− 4.5		0.628	0.252
	− 8.5		0.124	0.073
The last day of snowfall	− 2.6	0.05	0.836	0.275
	− 4.5		0.202	0.941
	− 8.5		0.231	0.202
Annual snowfall	− 2.6	0.054	0.867	0.677
	− 4.5		0.544	0.847
	− 8.5		0.005	0.934
Days of snowfall	− 2.6	0.303	0.295	0.351
	− 4.5		0.17	0.469
	− 8.5		0.044	0.292
Snowfall intensity	− 2.6	0.072	0.702	0.734
	− 4.5		0.717	0.747
	− 8.5		0.087	0.208
Maximum of daily snowfall	− 2.6	0.005	0.866	0.824
	− 4.5		0.871	0.344
	− 8.5		0.28	0.921

1.0 °C for RCP2.6, − 4.5 and − 8.5 under the 1.5 °C warming, and it will increase by approximately 11.71%, 9.06%, 12.54% per 1.0 °C for RCP2.6, − 4.5 and − 8.5 under an additional 0.5 °C global warming. The predicted increases in PA vary between the RCP scenarios considered and exhibit obvious spatial difference, showing an increase in all areas except part of southern UYRB. Relative to the baseline period, the frequency of trace, light and moderate precipitation days will decrease, however, that of heavy and intense precipitation days will increase for RCP2.6 under the 1.5 °C warming scenario. For RCP4.5, only the frequency of trace precipitation days will decrease by approximately 3 days, which is similar to that of RCP8.5. Under the 2 °C warming scenario, the frequency of trace precipitation will decrease by 3 days, 4 days and 5 days for RCP2.6, − 4.5 and − 8.5 relative to the baseline period, while the frequency of other precipitation days shows a slight increase for all RCPs. In general, the frequency of trace and light precipitation days was projected to decrease and the frequency of moderate and heavy days was projected to increase under both the 1.5 °C and 2 °C global warming scenarios, which means that the occurrence of trace and light precipitation events depends more heavily on global warming than the occurrence of other types of precipitation events (Ma et al. 2015; Zhang et al. 2013).

The ASF is projected to exhibit an overall decreasing trend in the UYRB under both 1.5 °C and 2 °C global warming scenarios. The rates of decrease are 0.6 mm/year for RCP2.6, 1.23 mm/year for RCP4.5, and 1.35 mm/year for RCP8.5 under the 1.5 °C global warming scenario,

which changes to 0.13, 0.31 and 0.79 mm/year under the 2 °C global warming scenario. The ASF will decrease by approximately 2.6%, 6.05% and 8.15% per 1.0 °C for RCP2.6, − 4.5 and − 8.5 under the 1.5 °C warming, and by 2.15%, 2.64% and 4.36% per 1.0 °C for RCP2.6, − 4.5 and − 8.5 under the 2 °C warming. Under all global warming scenarios, the ASF exhibits large and usually significant decreasing trend in most of the UYRB except for the northern end of the study area. For all scenarios, the ASF is predicted to exhibit a significant decreasing trend in most of the UYRB, with the largest variation occurring under the RCP4.5 scenario. The date of the first snowfall will delay with increasing temperature, while that of the last snowfall will advance. Under the 1.5 °C global warming scenario, the first snowfall is projected to occur a little earlier for RCP2.6 and to be delayed for the other RCPs, while the last snowfall is projected to occur a little earlier for all RCPs, with the largest advancement of 11 days for RCP4.5. Under the 2 °C global warming scenario, the first snowfall will delay by approximately 2, 2, and 5 days for RCP2.6, − 4.5 and − 8.5, and last snowfall will advance by approximately 14 days for RCP8.5, which is the largest, relative to the baseline period. Other types of snowfall indices show slight changes.

Overall, the increase of temperatures is projected to be associated with the increase of precipitation and the decrease of snowfall in the UYRB, which differ somewhat for the different RCPs considered. This study suggests that the precipitation in the UYRB will continue to increase and the snowfall will continue to decrease with increasing GMAT,

thereby increasing the probability of flooding in the study area.

References

Aerenson T, Tebaldi C, Sanderson B, Lamarque J-F (2018) Changes in a suite of indicators of extreme temperature and precipitation under 1.5 and 2 degrees warming. Environ Res Lett 13:035009. https://doi.org/10.1088/1748-9326/aaafd6

Cannon AJ, Sobie SR, Murdock TQ (2015) Bias correction of GCM precipitation by quantile mapping: how well do methods preserve changes in quantile and extremes? J Clim 28:6938–6959. https://doi.org/10.1175/JCLI-D-14-00754.1

Chaturvedi RK, Kulkarni A, Karyakarte Y, Joshi J, Bala G (2014) Glacial mass balance changes in the Karakoram and Himalaya based on CMIP5 multi-model climate projections. Clim Change 123:315–328. https://doi.org/10.1007/s10584-013-1052-5

Chen JL, Wilson CR, Ries JC, Tapley BD (2013) Rapid ice melting drives Earth's pole to the east. Geophys Res Lett 40:2625–2630. https://doi.org/10.1002/grl.50552

Chen J et al (2017) Assessing changes of river discharge under global warming of 1.5 °C and 2 °C in the upper reaches of the Yangtze River Basin: approach by using multiple-GCMs and hydrological models. Quatern Int 453:63–73. https://doi.org/10.1016/j.quaint.2017.01.017

Deng HJ, Pepin NC, Chen YN (2017) Changes of snowfall under warming in the Tibetan Plateau. J Geophys Res Atmos 122:7323–7341. https://doi.org/10.1002/2017JD026524

Dore MHI (2005) Climate change and changes in global precipitation patterns: what do we know? Environ Int 31:1167–1181. https://doi.org/10.1016/j.envint.2005.03.004

Eden JM, Widmann M, Grawe D, Rast S (2012) Skill, correction, and downscaling of GCM-simulated precipitation. J Clim 25:3970–3984. https://doi.org/10.1175/jcli-d-11-00254.1

Elliott J et al (2014) Constraints and potentials of future irrigation water availability on agricultural production under climate change. Proc Natl Acad Sci 111:3239

Friedlingstein P et al (2014) Persistent growth of CO2 emissions and implications for reaching climate targets. Nat Geosci 7:709. https://doi.org/10.1038/ngeo2248

Gao J, Sheshukov AY, Yen H, Douglas-Mankin KR, White MJ, Arnold JG (2019) Uncertainty of hydrologic processes caused by bias-corrected CMIP5 climate change projections with alternative historical data sources. J Hydrol 568:551–561. https://doi.org/10.1016/j.jhydrol.2018.10.041

Gemmer M, Fischer T, Jiang T, Su B, Liu LL (2010) Trends in precipitation extremes in the Zhujiang River Basin, South China. J Clim 24:750–761. https://doi.org/10.1175/2010JCLI3717.1

Gudmundsson L, Bremnes JB, Haugen JE, Engen Skaugen T (2012) Technical Note: Downscaling RCM precipitation to the station scale using quantile mapping—a comparison of methods. Hydrol Earth Syst Sci Discuss 9:6185–6201. https://doi.org/10.5194/hessd-9-6185-2012

Harder P, Pomeroy J (2013) Estimating precipitation phase using a psychrometric energy balance method. Hydrol Process 27:1901–1914. https://doi.org/10.1002/hyp.9799

Held IM, Soden BJ (2006) Robust responses of the hydrological cycle to global warming. J Clim 19:5686–5699. https://doi.org/10.1175/JCLI3990.1

Huang NE et al (1998) The empirical mode decomposition and the Hilbert spectrum for nonlinear and non-stationary time series analysis. Proc R Soc Lond Ser A Math Phys Eng Sci 454:903

Huang NE, Wu M-LC, Long SR, Shen SSP, Qu W, Gloersen P, Fan KL (2003) A confidence limit for the empirical mode decomposition and Hilbert spectral analysis. Proc R Soc Lond Ser A Math Phys Eng Sci 459:2317

Huang DQ, Zhu J, Zhang YC, Huang AN (2013) Uncertainties on the simulated summer precipitation over Eastern China from the CMIP5 models. J Geophys Res Atmos 118:9035–9047. https://doi.org/10.1002/jgrd.50695

Hulme M (2016) 1.5 °C and climate research after the Paris Agreement. Nat Clim Change 6:222. https://doi.org/10.1038/nclimate2939

IPCC (2013) Summary for policymakers. In: Stocker TF (ed) Climate change 2013: the physical science basis. Cambridge University Press, Cambridge, pp 3–29

IPCC (2018) Summary for Policymakers. In: Global warming of 1.5°C. World Meteorological Organization, Geneva

Ji Z, Kang S (2013) Projection of snow cover changes over China under RCP scenarios. Clim Dyn 41:589–600. https://doi.org/10.1007/s00382-012-1473-2

Karmalkar AV, Bradley RS (2017) Consequences of Global Warming of 1.5 degrees C and 2 degrees C for regional temperature and precipitation changes in the contiguous United States. PLoS ONE 12:e0168697. https://doi.org/10.1371/journal.pone.0168697

Khoi DN, Suetsugi T (2014) Impact of climate and land-use changes on hydrological processes and sediment yield—a case study of the Be River catchment, Vietnam. Hydrol Sci J 59:1095–1108. https://doi.org/10.1080/02626667.2013.819433

Kunkel KE, Palecki MA, Hubbard KG, Robinson DA, Redmond KT, Easterling DR (2007) trend identification in twentieth-century U.S. snowfall: the challenges. J Atmos Ocean Technol 24:64–73. https://doi.org/10.1175/jtech2017.1

Kunkel KE, Palecki M, Ensor L, Hubbard KG, Robinson D, Redmond K, Easterling D (2009) Trends in twentieth-century U.S. snowfall using a quality-controlled dataset. J Atmos Ocean Technol 26:33–44. https://doi.org/10.1175/2008jtecha1138.1

Lafon T, Dadson S, Buys G, Prudhomme C (2013) Bias correction of daily precipitation simulated by a regional climate model: a comparison of methods. Int J Climatol 33:1367–1381. https://doi.org/10.1002/joc.3518

Liu S, Deng S, Mo X, Yan H (2018) Indexing the relationship between polar motion and water mass change in a giant river basin. Sci China (Earth Science) 61:1065–1077. https://doi.org/10.1007/s11430-016-9211-2

Ma S, Zhou T, Dai A, Han Z (2015) Observed changes in the distributions of daily precipitation frequency and amount over China from 1960 to 2013. J Clim 28:6960–6978. https://doi.org/10.1175/JCLI-D-15-0011.1

Mankin JS, Diffenbaugh NS (2015) Influence of temperature and precipitation variability on near-term snow trends. Clim Dyn 45:1099–1116. https://doi.org/10.1007/s00382-014-2357-4

Meehl G, Bony S (2011) Introduction to CMIP5. Clivar Exchanges 16:4–5

Mitchell D, James R, Forster PM, Betts RA, Shiogama H, Allen M (2016) Realizing the impacts of a 1.5 °C warmer world. Nat Clim Change 6:735. https://doi.org/10.1038/nclimate3055

Moss RH et al (2010) The next generation of scenarios for climate change research and assessment. Nature 463:747. https://doi.org/10.1038/nature08823

Nelson GC et al (2014) Climate change effects on agriculture: economic responses to biophysical shocks. Proc Natl Acad Sci 111:3274

Ning L, Bradley RS (2015) Snow occurrence changes over the central and eastern United States under future warming scenarios. Sci Rep 5:17073. https://doi.org/10.1038/srep17073

O'Gorman PA (2014) Contrasting responses of mean and extreme snowfall to climate change. Nature 512:416. https://doi.org/10.1038/nature13625

Pepin N et al (2015) Elevation-dependent warming in mountain regions of the world. Nat Clim Change 5:424. https://doi.org/10.1038/nclimate2563

Peters GP et al (2012) The challenge to keep global warming below 2 °C. Nat Clim Change 3:4. https://doi.org/10.1038/nclimate1783

Ren Y, Liu S (2019) A simple regional snow hydrological process-based snow depth model and its application in the Upper Yangtze River Basin. Hydrol Res 50:672–690. https://doi.org/10.2166/nh.2019.079

Seneviratne SI et al (2018) Climate extremes, land–climate feedbacks and land-use forcing at 1.5°C. Philos Transact R Soc A Math Phys. Eng Sci. https://doi.org/10.1098/rsta.2016.0450

Seneviratne SI, Donat MG, Pitman AJ, Knutti R, Wilby RL (2016) Allowable CO2 emissions based on regional and impact-related climate targets. Nature 529:477. https://doi.org/10.1038/nature16542

Su B, Huang J, Zeng X, Gao C, Jiang T (2017) Impacts of climate change on streamflow in the upper Yangtze River basin. Clim Change 141:533–546. https://doi.org/10.1007/s10584-016-1852-5

Sun Y, Solomon S, Dai A, Portmann RW (2007) How often will it rain? J Clim 20:4801–4818. https://doi.org/10.1175/JCLI4263.1

Sun J, Wang H, Yuan W, Chen H (2010) Spatial-temporal features of intense snowfall events in China and their possible change. J Geophys Res Atmos. https://doi.org/10.1029/2009jd013541

Sun H et al (2018) Impacts of global warming of 1.5°C and 2.0°C on precipitation patterns in China by regional climate model (COSMO-CLM). Atmos Res 203:83–94. https://doi.org/10.1016/j.atmosres.2017.10.024

Teutschbein C, Grabs T, Karlsen RH, Laudon H, Bishop K (2015) Hydrological response to changing climate conditions: Spatial streamflow variability in the boreal region. Water Resour Res 51:9425–9446. https://doi.org/10.1002/2015WR017337

Trenberth KE, Dai A, Rasmussen RM, Parsons DB (2003) The changing character of precipitation. Bull Am Meteor Soc 84:1205–1218. https://doi.org/10.1175/BAMS-84-9-1205

Trenberth KE, Smith L, Qian T, Dai A, Fasullo J (2007) Estimates of the global water budget and its annual cycle using observational and model data. J Hydrometeorol 8:758–769. https://doi.org/10.1175/JHM600.1

Urry J (2015) Climate change and society. In: Michie J, Cooper CL (eds) Why the social sciences matter. Palgrave Macmillan UK, London, pp 45–59. https://doi.org/10.1057/9781137269928_4

van Vliet J et al (2012) Copenhagen accord pledges imply higher costs for staying below 2°C warming. Clim Change 113:551–561. https://doi.org/10.1007/s10584-012-0458-9

Wang L, Chen W (2013) A CMIP5 multimodel projection of future temperature, precipitation, and climatological drought in China. Int J Climatol 34:2059–2078. https://doi.org/10.1002/joc.3822

Wu Z, Huang NE (2009) Ensemble emperical mode decomposition: a noise-assisted data analysis method. Adv Adapt Data Anal 01:1–41. https://doi.org/10.1142/s1793536909000047

Xu Z, Qian Y (2005) Climate effect of 100 hPa easterly air flow in tropical (I): its relationship with climate anomalies in South China. Plateau Meteorol 24:378–387

Xu Y, Xu C (2012) Preliminary assessment of simulations of climate changes over China by CMIP5 multi-models. Atmos Ocean Sci Lett 5:489–494. https://doi.org/10.1080/16742834.2012.11447041

Xu Y, Xu C, Gao X, Luo Y (2009) Prpjected changes in temperature and precipitation extremes over the Yangtze Rover Basin of China in the 21st century. Quatern Int 208:44–52. https://doi.org/10.1016/j.quaint.2008.12.020

Yang P, Xia J, Zhang Y, Hong S (2017) Temporal and spatial variations of precipitation in Northwest China during 1960–2013. Atmos Res 183:283–295. https://doi.org/10.1016/j.atmosres.2016.09.014

Zhang J (2013) Evaluation and projection of temperature and precipitation over Yangtze River Basin on modeling data from CMIP3/5 and CCLM models. Thesis, Nanjing University of Information & Technology

Zhang X, Wan H, Zwiers FW, Hegerl GC, Min S-K (2013) Attributing intensification of precipitation extremes to human influence. Geophys Res Lett 40:5252–5257. https://doi.org/10.1002/grl.51010